HHS Public Access

Author manuscript

Exp Eye Res. Author manuscript; available in PMC 2021 July 01.

Published in final edited form as:

Exp Eye Res. 2020 July ; 196: 108049. doi:10.1016/j.exer.2020.108049.

Functional, Structural, and Molecular Identification of Lymphatic Outflow from Subconjunctival Blebs

Goichi Akiyama[a,b], **Sindhu Saraswathy**[a], **Thania Bogarin**[a], **Xiaojing Pan**[c], **Ernesto Barron**[a], **Tina T. Wong**[d], **Mika K. Kaneko**[e], **Yukinari Kato**[e,f], **Young Hong**[g], **Alex S. Huang**[a]

[a]Doheny Eye Institute and Department of Ophthalmology, David Geffen School of Medicine at UCLA, Los Angeles, CA, USA

[b]Jikei School of Medicine, Tokyo, Japan

[c]Qingdao Eye Hospital, Shandong Eye Institute, Shandong First Medical University, Qingdao, China

[d]Singapore National Eye Center and Singapore Research Institute, Singapore, Singapore

[e]Tohoku University Graduate School of Medicine, Miyagi, Japan

[f]New Industry Creation Hatchery Center, Tohoku University, Miyagi, Japan

[g]Division of Plastic and Reconstructive Surgery, Department of Surgery, Norris Comprehensive Cancer Center Keck School of Medicine, University of Southern California, Los Angeles, CA, USA

Abstract

The purpose of this study is to evaluate outflow pathways from subconjunctival blebs and to identify their identity. Post-mortem porcine (n = 20), human (n = 1), and bovine (n = 1) eyes were acquired, and tracers (fluorescein, indocyanine green, or fixable/fluorescent dextrans) were injected into the subconjunctival space to create raised blebs where outflow pathways were visualized qualitatively and quantitatively. Rodents with fluorescent reporter transgenes were imaged for structural comparison. Concurrent optical coherence tomography (OCT) was obtained to study the structural nature of these pathways. Using fixable/fluorescent dextrans, tracers were trapped to the bleb outflow pathway lumen walls for histological visualization and molecular identification using immunofluorescence against lymphatic and blood vessel markers. Bleb outflow pathways could be observed using all tracers in all species. Quantitative analysis showed that the nasal quadrant had more bleb-related outflow pathways compared to the temporal quadrant (nasal: 1.9 +/− 0.3 pathways vs. temporal: 0.7 +/− 0.2 pathways; $p = 0.003$). However, not all blebs resulted in an outflow pathway (0-pathways = 18.2%; 1-pathway = 36.4%; 2-pathways = 38.6%; and 3-pathways = 6.8%). Outflow signal was validated as true luminal pathways using optical coherence tomography and histology. Bicuspid valves were identified in

Corresponding Author: Alex Huang, MD/PhD, Doheny Eye Institute, Department of Ophthalmology, David Geffen School of Medicine, University of California, Los Angeles, 1355 San Pablo Street, Los Angeles, CA 90033, Ahuang@Doheny.org, Phone: 323-442-6436; Fax: 323-442-6688.

the direction of flow in porcine eyes. Immunofluorescence of labeled pathways demonstrated a lymphatic (Prox-1 and podoplanin) but not a blood vessel (CD31) identity. Therefore, subconjunctival bleb outflow occurs in discrete luminal pathways. They are lymphatic as assessed by structural identification of valves and molecular identification of lymphatic markers. Better understanding of lymphatic outflow may lead to improved eye care for glaucoma surgery and ocular drug delivery.

Keywords

Conjunctiva; Lymphatics; Aqueous Outflow; Glaucoma Surgery; Blebs

1. Introduction

Native aqueous humor outflow (AHO) occurs in the eye via two pathways (conventional and unconventional) (Huang and Weinreb, 2017; Johnson, 2006). However, an alternative pathway exists as a result of glaucoma surgery to lower intraocular pressure (IOP). This occurs in the subconjunctival space and is accessed during bleb-creating surgeries such as trabeculectomies (Gedde et al., 2018), glaucoma drainage devices (GDDs) (Gedde et al., 2018), and in some of the new Minimally Invasive Glaucoma Surgeries (Green et al., 2018; Lenzhofer et al., 2018a) (MIGS; Xen and Preserflo). While the subconjunctival aqueous outflow pathway is artificially created during glaucoma surgery, given its important role in glaucoma treatment, it deserves study as a way to improve AHO and to lower IOP.

Blebs are essentially fluid filled blisters or sacs located under the conjunctiva and above the scleral surface. Blebs can form naturally (termed chemosis) in certain pathological situations such as systemic fluid overload, post-surgical, or during ocular surface infection/inflammation (Glauser, 1974; Michael et al., 2016; Shoukath et al., 2017). Blebs can also be artificially created when medicines are injected subconjunctival to prophylax against infection after surgery and to treat scleritis and macular edema in patients (Gower et al., 2017; Sohn et al., 2011; Thach et al., 1997). Surgically, blebs are crafted to create a low-resistance AHO pathway to decrease IOP in trabeculectomies (Gedde et al., 2018), GDDs (Gedde et al., 2018), or subconjunctival MIGS (Green et al., 2018; Lenzhofer et al., 2018a). We predict that for a bleb to survive, a) the pathway for aqueous inflow must be stable, b) the bleb itself cannot scar down, and c) aqueous must have the ability to exit the bleb.

The major effort in studying and improving blebs and bleb surgeries has focused on the first two requirements above. By using artificial implants in GDDs and subconjunctival MIGS, the pathway from the anterior chamber to the bleb becomes stable. Then the introduction of anti-fibrotics (mitomycin-C [MMC] and 5-fluorouracil [5FU]) (Palanca-Capistrano et al., 2009) has been instrumental in enhancing bleb survival in both animal models and human surgeries. These agents non-specifically ablate dividing cells to limit fibroblastic activity and extracellular matrix deposition that result in a scarred bleb (Lama and Fechtner, 2003). Unfortunately, research into more specific agents that target single regulatory points in scar-related molecular pathways, such as TGF-β, have been less successful (Khaw et al., 2007). Nevertheless, despite these advances, all glaucoma surgeons have seen surgical cases where

the bleb appears structurally present, a cavity could even be demonstrated using imaging tools such as optical coherence tomography (OCT), but IOP is still elevated. Thus, aqueous is entering the bleb but apparently cannot escape.

The biology of how fluid exits a bleb in the subconjunctival space has not been studied enough. It was noted decades ago that, after subconjunctival hemorrhage, blood resolved with linear sausage-shaped patterns (Grüntzig and Hollmann, 2019). Ink clearance from scleral tattooing can do the same (Grüntzig and Hollmann, 2019). Injection of tracers directly under the conjunctiva have more clearly demonstrated these bleb outflow pathways. These experiments have been performed in enucleated and live eyes in non-primate vertebrates (Yu et al., 2009), non-human primates (Guo et al., 2012; Yu et al., 2009), and humans (Benedikt, 1976; Freitas-Neto et al., 2015). Based on their appearance and by virtue of the known presence of lymphatics in the subconjunctival space, these pathways have been hypothesized to be lymphatics. This has not been proven though by structural or molecular study of the literal pathways that were observed. Alternatively, another option is that local blood vessels represent these pathways and remove agents delivered into the subconjunctival space.

Aqueous angiography is a tracer-based method designed to visualize AHO from the conventional AHO pathways (Huang et al., 2018; Huang et al., 2016a; Xie et al., 2019). Aqueous angiography was developed in the laboratory using post-mortem animal and human eyes. Aqueous angiography was validated as representing conventional AHO using immunofluorescent and structural methods (Huang et al., 2017a; Saraswathy et al., 2016). Aqueous angiography was translated to the operating room for living non-human primates (Huang et al., 2017c) followed by imaging in humans undergoing clinically-indicated cataract surgery (Huang et al., 2017b). Aqueous angiography has demonstrated segmental, pulsatile, and dynamic AHO behaviors (Huang et al., 2017b; Huang et al., 2017c). Aqueous angiography has shown, in laboratory (Huang et al., 2016b; Huang et al., 2016c) and in live glaucoma patients undergoing trabecular MIGS (Huang et al., 2019), that surgery can lead to many types of angiographic AHO improvement.

Because of our tracer-based outflow research experience for conventional/trabecular outflow, we modify aqueous angiography to perform ocular surface lymphangiography (OSL) to study subconjunctival AHO. We start with the previous hypothesis that subconjunctival outflow is lymphatic in nature. After tracer-identification of these pathways in post-mortem eyes of various species, we specifically isolate and study these pathways using molecular and structural assessment tools to determine their identity. By better understanding bleb biology, and in particular bleb outflow, improved glaucoma surgeries can be designed for enhanced IOP lowering outcomes.

2. Methods

2.1. Study Materials

Post-mortem and enucleated eyes were used for this study. Porcine (n = 20) and bovine (n = 1) eyes were obtained from SiouxPreme Packing Company (Sioux Center, IA; within 48 hours of death) and Manning Beef LLC (Pico Rivera, CA; within 6 hours of death),

respectively. Of the 20 porcine eyes, 11 received indocyanine green (ICG) for counting bleb-related outflow pathways, 1 received ICG for optical coherence tomography (OCT), 3 received fluorescein for videos or still photography, and 5 received fixable/fluorescent dextrans for some combination of OCT, excisional, luminal dimension measurements, or immunofluorescent studies. The human eye (n = 1; 54-year-old male; right eye; cause of death: cardiac arrest) was obtained from OneLegacy Eye Bank (Los Angeles, CA; within 36 hours of death). Rodent eyes are described below.

2.2. Ocular Surface Lymphangiography

Eyes (porcine/bovine/human) were procured, excess tissue was trimmed, and the eyes were pinned to Styrofoam. Eyes with visible damage to the conjunctiva near the limbus were excluded. Damage only occurred in porcine eyes and represented less than 10% of eyes obtained from the abattoir. Tracers included fluorescein, indocyanine green, and fluorescent dextrans. For fluorescein, a 25% stock (Akorn; Lake Forest, IL) was diluted at room temperature (RT) in balanced salt solution (BSS) to 2.0%. ICG (Sigma I2633; St. Louis, MO) was dissolved with deionized water into a 2% stock solution, and this stock was further diluted in BSS to 0.4%. Fluorescent FITC-dextrans (Thermo-Fisher; Waltham, MA; D7136) were diluted to 2.5 mg/ml in BSS, and a 500 kilodalton size was purposefully chosen given the large molecular weight and lesser chance for leakage out of lymphatics. The dextrans were additionally fixable due to an attached lysine moiety so that they could be trapped to nearby tissue in the presence of an aldehyde fixative. In each case, 0.12 forceps were used to raise the conjunctiva. Using a 30-gauge needle, the conjunctiva was pierced just until the bevel and needle lumen were fully buried, and 100 microliters of the tracer were injected into the subconjunctival space to create a bleb for imaging. In quantitative experiments, four separate ICG blebs (superior, inferior, nasal, and temporal) were created in eleven porcine eyes.

The imaging protocol utilized a 12 mega-pixel digital camera (Apple, Cupertino, CA) or the Heidelberg Spectralis (HRA+OCT; Heidelberg Engineering, Heidelberg, Germany) for pictures and videos. Videos were cropped and motion corrected (Vegas Pro 13, Sony; New York, USA). Natively, fluorescein is orange, and ICG is dark green. Thus, fluorescein images were taken with a digital camera. The ICG images were taken using the confocal scanning laser ophthalmoscopic (CSLO) infrared function on the Spectralis. For fluorescent dextrans, a standard pre-tracer background image was taken using the Spectralis CSLO angiographic FITC setting with a sensitivity setting where the background appeared black. The FITC settings were: excitation wavelength = 486 nm and transmission filter set at > 500 nm. On the Spectralis, images were either taken with a 55-degree lens using a 25 diopter focus or the anterior segment lens.

2.3. Quantitative Analyses

In eleven porcine eyes, 100 microliters of ICG was injected subconjunctival in different locations (superior, inferior, nasal, and temporal). The number of outflow pathways that were visualized were counted. To test whether subconjunctival tracer injection in certain locations (superior/inferior/temporal/nasal) were better or worse for accessing an outflow pathway, a Kruskal-Wallis test (SAS, version 9.3) was performed. The Kruskal-Wallis test is

a non-parametric statistical test used to detect mean differences across groups. It was chosen in this analysis because of the relatively small sample size, which does not have enough statistical power to check the normal distribution assumption used in ANOVA. Here, the null hypothesis was that the number of outflow pathways across all quadrants was equal. Rejecting the null hypothesis would mean that there was an overall statistically significant difference in the number of bleb-related outflow pathways across quadrants. Since this ended up being the case, to determine which quadrant had more or fewer outflow pathways, the different quadrants (inferior vs. temporal, inferior vs. superior, inferior vs. nasal, temporal vs. superior, temporal vs. nasal, and superior vs. nasal) were compared using six t-tests. As each eye generated data points for superior, inferior, nasal, and temporal quadrants, paired t-tests were used. To preserve an overall type-1 error rate of 0.05 and to statistically account for multiple comparisons, results were considered significant across the 6 comparisons only if $p < 0.05/6 = 0.008$ (Bonferroni correction; $p <$ [acceptable p-value]/[number of comparisons]). All quantitative data are shown as mean +/− SEM.

2.4. Anterior Segment Optical Coherence Tomography (OCT)

Anterior segment OCT (anterior segment module, Scleral Mode [Spectralis, Heidelberg Engineering; Germany]) was also conducted concurrently with ocular surface lymphangiography. In angiographically positive regions, single line scans with a 15-degree scan angle (3.9-micron axial and 11-micron lateral resolution; ~ 4.5 mm) were taken with oversampling (automated real time = 20). Size measurements were made with in-built calipers. Spectralis comparisons between OCT and CSLO images were performed using in-built rulers and sliders. The accuracy of this cross-modality comparison between the Spectralis OCT and CSLO has been reported at ~14 microns which is near the lateral resolution of the OCT itself (~14 microns) (Barteselli et al., 2013). This is due to the Spectralis TruTrack system where the CSLO image is mapped at over 1000 points using one light beam during CSLO imaging and mapped as a reference to the second beam to acquire the OCT. This mitigates eye motion artifact and ensures accurate point-to-point correlations between the OCT and CLSO images. Given such high accuracy and as an example, retinal lesions can even be mapped and compared between the CSLO and OCT images longitudinally with images acquired over 1 year apart from the same subject (Huang et al., 2012).

2.5. Rodent studies

To provide a comparison, adult mice and rats with fluorescent reporter lymphatic genes were studied. Experiments complied with the Association for Research in Vision and Ophthalmology (ARVO) Statement for Use of Animals in Ophthalmic and Vision Research. Approval was obtained from the Institutional Animal Care and Use Committees (IACUC) at USC (PI: YK Hong) and UCLA (PI: Huang). Mice and rats were housed and raised in air-filtered clear cages in a 12-hour light/dark cycle environment and fed ad libitum. Prox1-EGFP mouse (Choi et al., 2011) and Prox1-EGFP rat (Jung et al., 2017) were previously reported where lymphatic vessels could be conveniently visualized. All mice were maintained as outbred strains, whereas inbred Prox1-EGFP rats (Sprague Dawley) were used for this study. One rat and one mouse were euthanized by carbon dioxide asphyxiation followed by cervical dislocation, and the eyes were harvested. Eyes were fixed in 4%

paraformaldehyde (PFA) at 4°C for 2–4 hours. The eyes were cut in half and the lens and iris removed. The anterior half was then flattened using radial incisions, placed on a slide, and mounted with a cover slip. Fluorescent images were captured using a Zeiss ApoTome Microscope (Zeiss AxioVision software).

2.6. Histology and Immunofluorescence

After injection of fluorescent and fixable dextran and visualization of the bleb-related outflow pathway, the entire region of porcine eyes (n = 3) that included the bleb and outflow pathways (from conjunctiva to sclera) were carefully excised using scissors and placed in PFA for 15 minutes at RT followed by overnight at 4°C to trap the tracer. The tissue block was then marked for orientation and placed in Tissue-Tek (Sakura; Torrance, CA), frozen under liquid nitrogen, and 8-micron sections cut (Thermo Scientific CryoStar NX70) onto Superfrost slides (Fisher; Pittsburgh, PA). After blocking sections with 5% bovine serum albumin in phosphate buffered saline (PBS) and permeabilization with 0.3% Triton X-100 in PBS, sections were incubated with primary antibody at 4°C overnight. Antibodies included: a) mouse monoclonal anti-porcine podoplanin (10 μg/ml; pMab-213 provided by Y. Kato (Kato et al., 2019)), b) rabbit polyclonal anti-mouse CD31 (1:20; Abcam ab28364, Cambridge, UK), c) goat polyclonal anti-human Prox-1 (1:100; R&D Systems AF2727, Minneapolis, MN), and d) anti-goat, anti-mouse, and anti-rabbit Texas red secondary antibodies (1:100; Thermo-Fisher). Slides were mounted with 4’6-diamidino-2-phenylindole (DAPI) containing mounting medium (Vector Lab; Burlingame, CA) and viewed under a Keyence BZ-X700 digital imaging microscope (Keyence; Chicago, IL). Sections were imaged using a 10x or 20x plan-fluor lens. All images were taken using identical settings for illumination and image capture sensitivity (Keyence imaging software v.f1.51). For FITC-dextrans (EX BP 470/30, DM 495, EM BP 520/35), DAPI (EX BP 360/40, DM 400, EM BP 460/50), and Texas Red (EX BP 560/40, DM 565, BP 630/75) appropriate filters were used. Identification of above lymphatics followed consensus guidelines, including the use of the above markers, more than one marker, structural analyses, and assessment of blood vessel markers (Schroedl et al., 2014). This was done for additional assurance even though the guidelines exactly stated that these steps were not required for the conjunctiva since lymphatic presence has already been well-documented (Schroedl et al., 2014).

2.7. Two-photon Microscopy

In one case, whole-labeled porcine tissue was imaged by two-photon microscopy on a Zeiss 710 NLO (Carl Zeiss, Ag; Oberkochen, Germany) equipped with a chameleon multiphoton laser (Coherent, Santa Clara; CA, USA). Conjunctiva where the outflow pathway was located was dissected from the underlying sclera and placed on a glass bottom dish (P35G-1.5–14-C; MatTek corporation, Ashland, MA) along with a drop of PBS. A 10x Neofluar lens NA 0.3 was used to focus an 850 nm wavelength laser to excite the fluorescent dextrans. A 500–550 nm bandpass filter was used to collect the fluorescent signal. Images (1024 ×1024 pixels and a 16-bit grayscale resolution) were captured using the Zeiss Zen software.

3. Results

Various tracers were injected subconjunctival in enucleated post-mortem eyes of several species (porcine, bovine, and human). Video recordings from pig eyes showed that after bleb formation, distinct tracer-based linear extensions could arise from some blebs (Clip 1; arrows) but not others (Clip 2). Comparing different tracers, these extensions could be seen using fluorescein (Fig. 1A), ICG (Fig. 1B/C), and fluorescent dextrans (Fig. 1D/E). Fluorescein and ICG have native coloration so that they could be visualized with standard photography or confocal laser scanning ophthalmoscopy, without fluorescent laser excitation. Fluorescein was also noted to leak, and this is consistent with its known small molecular weight (332 g/mol or daltons). ICG is however larger (774 g/mol or daltons) and can even be protein bound to be yet larger. Therefore, ICG and very large fluorescent dextrans (500 kilodaltons) gave sharper and more defined images of the outflow pathways. Across species (porcine [Fig. 1 A/B/D], bovine [Fig. 1C], and human [Fig. 1E]), bleb-related outflow pathways were similar. Overall, these outflow pathways were qualitatively different from veins which take typical linear and Y-shaped patterns (Gaasterland and Pederson, 1983). Instead, bleb-related outflow pathways were nonlinear and irregular. Also, careful observation showed a variegated signal where along the outflow pathways, brighter regions were intermixed with darker bands (Fig. 1D/E; white arrows). Zoomed-in images for Fig. 1D/E showed the darker bands (Fig. 1F/G white arrows, respectively) more clearly. Given greatest access to porcine eyes, most of the subsequent quantitative, structural, and molecular studies focused on this species.

The number of outflow pathways that arose from subconjunctival blebs were quantified. Four blebs were created in different locations (superior, inferior, temporal, and nasal) in eleven separate eyes. Each bleb was created with 100 microliters of ICG, and the total number of extending outflow pathways were counted, showing a different distribution in each quadrant (Fig. 2A). On average, the number of pathways per bleb location were: superior (1.5 +/− 0.3; mean +/− SEM), inferior (1.3 +/− 0.2), temporal (0.7 +/− 0.2), and nasal (1.9 +/− 0.3) (Fig. 2B). Regardless of location, across all blebs, zero-pathways were seen in 18.2% (8 of 44), 1-pathway was seen in 36.4% (16 of 44), 2-pathways were seen in 38.6% (17 of 44), and three-pathways were seen in 6.8% (3 of 44) of blebs (Fig. 2C). To determine if access to outflow pathways was non-uniform around the limbus, a Kruskal-Wallis test was performed with the null hypothesis that there was no overall mean difference among the quadrants. The null hypothesis was rejected (H-statistic: 10.03; $p = 0.018$). Thus, bleb-related outflow pathways were not uniform around the limbus, and because of this pair-wise t-tests were performed comparing all combinations. Given multiple comparisons, a Bonferroni correction was made such that statistical significance was only considered for $p < 0.008$. There was only a statistically significant difference comparing nasal vs. temporal ($p = 0.003$). The results for the other comparisons were non-significant: superior vs. temporal ($p = 0.09$), superior vs. nasal ($p = 0.30$), superior vs. inferior ($p = 0.64$), nasal vs. inferior ($p = 0.05$), and temporal vs. inferior ($p = 0.08$).

To determine the nature of these outflow pathways, structural and molecular studies were performed. First, in one porcine eye, subconjunctival fluorescent dextran was injected to create a bleb (Fig. 3A; black asterisk) with a superiorly-directed outflow pathway (Fig. 3A;

blue arrow). Then the conjunctiva where the bleb and outflow pathway was located was excised (Fig. 3B). The residual and underlying bare sclera showed continued fluorescence where the bleb was once located (Fig. 3C; black asterisks). However, the previous fluorescent outflow pathway was gone, and instead a black linear structure was seen but that did not carry a fluorescent signature (Fig. 3C; red arrow). This could represent an artery or vein, not associated with fluid flow off the bleb. Focusing on the excised piece of conjunctiva (Fig. 3B), under fluorescent excitation (Fig. 3D), both the bleb (Fig. 3D; black asterisk) and original outflow pathway (Fig. 3D; blue arrow) were re-visualized. This demonstrated that the outflow pathway was located within the excised conjunctival piece.

Concurrent optical coherence tomography (OCT) was then performed on the bleb-related outflow pathways. OCT, perpendicular to an outflow pathway, showed a distinct and luminal structure that corresponded exactly to the angiographic outflow pathway location in the eye (Fig. 4A/B). OCT comparison to angiography is possible because of the Spectralis dual-beam TruTrack system that ensures highly accurate point-to-point correlations between the OCT and CLSO images (Barteselli et al., 2013). The bleb-related outflow pathway's relatively superficial location supported the results from the excisional experiment result (Fig. 3) and a conjunctival origin for these pathways. OCT along a short-segment of an outflow pathway also showed a luminal structure whose length exactly matched the extent of the fluorescent outflow pathway itself (Fig. 4C/D; blue and orange arrows on the angiographic image matched exactly the location of the same colored arrows on the OCT). Other luminal pathways were seen as well. In some cases, OCT across an angiographic pathway showed the lumen (Fig. 4E/F; yellow arrows) next to another lumen (Fig. 4E/F; red arrows) that did not carry angiographic tracer signal. Note that this non-angiographic lumen was smaller in size compared to the lumen associated with the angiographic signal. (Fig. 4F; red arrow vs. yellow arrow). This may reflect increased intraluminal pressure which one would expect to be higher in the fluorescent pathway since actual tracer was injected. Note that in the excised piece of conjunctiva (Fig. 4G/H), OCT in the same approximate location gave the same arrangement. There were two lumens, and one matched the angiographic signal but the other did not. Further, both lumens were of approximately the same size after the conjunctiva was excised. This may be expected as excising and opening the conjunctiva would remove any pressure head initially driven by tracer injection. Across five eyes receiving fluorescent dextran blebs, 14 pathways were visualized with OCT demonstrating luminal dimensions of 215.9 +/− 24.4 microns (mean +/− SEM; range: 110 to 455 microns) horizontal and 102.4 +/− 7.8 microns (range: 37 to 136 microns) vertical. Lastly, detailed OCT on the bleb and outflow pathway junction demonstrated a hole (159 × 34 microns) through which tracer could exit the bleb (Fig. 4I/J).

Structural studies supported a lymphatic identity. Given the fluorescent signal, a small piece of the excised porcine conjunctiva with an outflow pathway but away from the bleb (Fig. 1D area pointed out by white arrows which is the tissue that was also shown in Fig. 3B) was submitted for two-photon microscopy. Higher magnification imaging again demonstrated irregular structures but now with blind ends (Fig. 5A; white arrows) which may represent lymphatic capillary tips. The outflow pathways then grew into larger extensions which could represent pre-collector lymphatics followed by even bigger pathways notable for bright fluorescent regions (Fig. 5A) separated by dark bands (Fig. 5A; orange arrow). This

qualitative appearance of dark bands using two-photon microscopy was very similar to the results from the Spectralis above (Fig. 1D–G). To further delve into this, these images were compared to lymphatic appearance from lymphatic reporter mouse (Choi et al., 2011) and rat (Jung et al., 2017). These rodents express GFP under a Prox-1 promoter (Fig. 5B/C), and the natively fluorescent subconjunctival lymphatics also show a variegated signal with bright and dark regions with focal bright spots known to represent valves (Choi et al., 2011) (Fig. 5B/C). Comparing ocular surface lymphangiography to the reporter rodents, the focal dark regions in ocular surface lymphangiography may correspond to the focal bright region in the reporter rodents and thus be valves.

Thus, we tested for the presence of valves using OCT on ocular surface lymphangiography with an emphasis on the focal dark regions. In porcine eyes, the presence of bicuspid valves was confirmed using OCT (Fig. 5D–F). After creation of the bleb (Fig. 5D), tracer flow exited in the direction denoted by the sequence of arrows (Fig. 5E; red, blue, and then yellow arrows). As this pathway was more linear, OCT was performed to capture the entire pathway (Fig. 5F). The color arrows on the OCT (Fig. 5F) corresponded to the exact location of the same color arrows of the angiographic image (Fig. 5E). Thus, the OCT demonstrated conjunctival bicuspid valves that lined correctly with the direction of flow (Fig. 5F). The location of the valves also matched that of the dark bands (Fig 5D/F; white arrows). Lymphatics (including in the conjunctiva) are known to have valves (Gong et al., 2018; Schulte-Merker et al., 2011). Measuring valve leaflets (n = 6 leaflets; Fig. 5) from the base to the valve tip, the average leaflet length was 151.7 +/− 14.9 microns (mean +/− SEM).

To determine the molecular characteristic of bleb-related outflow pathways, immunofluorescence was performed. However, the first and critical step was to be able to identify the exact outflow pathways seen on the angiographic image on a histological section. Thus, this experiment utilized the blebs created by the fluorescent and fixable dextrans. A lysine moiety, attached to the dextran, allowed for trapping of the tracer to the luminal walls of the pathways that it flowed through. After creation of the fluorescent bleb and outflow pathway, 4% PFA was given to trap the tracer in place. Histological section identified the lumen tracer coating the lumen wall (Fig. 6A/D/G/J/M). Co-immunofluorescence against Prox-1 and podoplanin demonstrated co-labeling of these lumens with lymphatic markers (Fig. 6B/E/H/K). Note that other lymphatics could be seen nearby the bleb-related outflow pathway that did not carry the fluorescent dextran tracer (Fig. 6K/L; white arrows). These lymphatics presumably drain nearby regions outside of where the bleb was created. In some cases, dextran- and lymphatic marker-positive debris-like material could be seen within the lumens. Their identity is unclear and maybe valvular or vessel lumen lining tissue that migrated into the lumen during sectioning steps. Then, immunofluorescence against blood vasculature (CD31 is highly expressed in blood vessels and only weakly in lymphatics (Baluk et al., 2007)) showed blood vessels in the section that did not co-localize with the bleb-related fluorescent dextran outflow pathway (Fig. 6M–O), indicating that blood vessels are not draining the blebs..

4. Discussion

Tracer-based studies where labeled substances were delivered into the subconjunctival space have been performed for many years (Benedikt, 1976; Freitas-Neto et al., 2015; Grüntzig and Hollmann, 2019; Yu et al., 2009). Across many species (including live humans) and conditions (via glaucoma surgeries or direct injection into the subconjunctival space) distinct outflow pathways have been observed (Benedikt, 1976; Freitas-Neto et al., 2015; Grüntzig and Hollmann, 2019; Yu et al., 2009). These pathways have long been hypothesized and assumed to be lymphatics because a) subconjunctival lymphatics exist (Guo et al., 2012) and because b) lymphatics should drain extracellular spaces in the body. However, while long-studied and potentially clinically important, the lymphatic identity of fluid outflow pathways from the subconjunctival space has not been definitively proven. The results herein provide direct evidence of a lymphatic identity using a multi-model approach starting with fluorescent tracers that can be visualized after subconjunctival injection. After identification of the pathways, simultaneous anterior segment optical coherence tomography (OCT) on these exact structures demonstrated lumens and in particular biscuspid valves in the direction of flow. One of the hallmarks of lymphatics is that they have valves (Gong et al., 2018; Schulte-Merker et al., 2011), and the valve leaflet size in this work (~150 microns) matched well with published lymphatic valve leaflet measurements (~100 microns (Swartz, 2014)). Co-immunofluorescence against two lymphatic markers further confirmed a molecular lymphatic identity. Thus, we not only observed outflow pathways for subconjunctival outflow, but we simultaneously studied the identity of these pathways using structural (OCT) and molecular (immunofluorescence) methods.

The clinical implications of these findings are important and can be directed at drug delivery or glaucoma surgery. Drug delivery that is better than topical drop application has long been sought. The disadvantages of topical drug delivery include the need for adherent and persistent (Cairns, 1968) use, the need to bypass epithelial barriers (Pleyer et al., 2013), and the inability to maintain long-standing high-concentration drug depots. Current modern drug-delivery approaches include intravitreal (Martin et al., 2011) and intracameral injections. Limitations of intraocular injections include pain (Shiroma et al., 2017) and the risk of endophthalmitis (Menchini et al., 2018). Thus, the subconjunctival space has also been studied as an alternative drug delivery site. This space is highly accessible. Drugs have been proven to enter the eye from this space (Raghava et al., 2004; Weinreb, 2001) and can even reduce IOP (Pitha et al., 2018). Special formulations have been proposed to enhance the longevity of drugs delivered there (Wong et al., 2014). Clinically, subconjunctival (Sohn et al., 2011) or subtenon (Thach et al., 1997) steroids are injected for inflammatory conditions. After surgery, subconjunctival steroids and antibiotics can also be given (Gower et al., 2017). However, surgeons have long known that while a bleb is initially formed by the drug injection, by the next morning the physical bleb is gone. Thus, subconjunctival drugs must flow out of and exit this space. Future strategies designed to limit lymphatics or to target drug injections to where there are fewer lymphatics could enhance the subconjunctival space as a better drug delivery location.

Glaucoma surgery can also benefit from a better understanding of subconjunctival lymphatics and bleb outflow. The relationship between lymphatics and blebs are in an early

stage of research. It has been shown that tracer flow from Xen blebs move into lymphatic-like structures (Yu et al., 2009). Xen blebs with luminal openings that look like lymphatics seen in this report are associated with greater IOP reduction (Lenzhofer et al., 2018b). Bleb histology from failed trabeculectomy blebs show a complete lack of lymphatics compared to normal conjunctiva (Bouhenni et al., 2016). Peri-failed bleb conjunctiva shows intermediate lymphatic presence (Bouhenni et al., 2016). In trabeculectomy, better IOP lowering is also seen in cases when blebs show lymphatic-like outflow pathways during tracer studies (Khoo et al., 2019). Thus, lymphatics seem to be associated with clinical bleb outflow with a lack of lymphatics being associated with failure. All of this is important because glaucoma surgeons are familiar with cases of bleb-related surgeries which successfully create an extraocular reservoir (implying adequate inflow), but IOP is not reduced (implying inadequate outflow). A complex relationship between bleb connective tissue and lymphatics likely forms post-operative, and variability here may influence surgical success. Therefore, future study of how these lymphatics respond to surgery may lead to strategies for improving IOP-lowering surgical outcomes.

The qualitative and quantitative results of lymphatic bleb drainage in this report provide important clues about how lymphatics may drain the subconjunctival space. Qualitatively, the lymphatic structural evaluation in rodents showed numerous lymphatics while injection studies only accessed 0–3 lymphatic pathways (Fig. 2). The structural result is consistent with Guo et al.'s results that showed numerous and widespread subconjunctival lymphatics in non-human primates (Guo et al., 2012). In tracer studies, since lymphatics only drain at their tips, only the lymphatics that drain where the tracers are delivered are expected to be visualized. Further, most bleb-related outflow pathways were seen nasal, but this was only statistically significant compared to the temporal quadrant. Overall, these findings also agree with preliminary data that we have obtained in our mouse lymphatic reporter model (manuscript under review). Developmentally, the subconjunctival lymphatics developed from a nasal direction before wrapping around the limbus to end on the temporal side of the eyes, resulting in a final adult nasal>temporal lymphatic distribution. Further, when tracer was injected under the conjunctiva (temporal vs. nasal side of the eye), the tracer cleared to a greater extent on the nasal side where there were more lymphatics. This gives functional importance. In the future, studied in humans, with greater power, and with a focus on individual variation, there may be locations with the greatest lymphatic density and where bleb-related glaucoma surgeries could be best targeted. Lastly, there was an uneven distribution of outflow pathways arising from the blebs studied. Approximately, 36% of blebs showed one outflow lymphatic, while ~39% showed two, ~7% showed three, and ~18% showed none. This is important because this means that not every bleb investigated in this study accessed lymphatic outflow. Some accessed a lot. The features that govern whether a bleb in a certain location accesses lymphatics need to be better understood. If these features could be pre- or intra-operatively identified, surgical blebs could be placed in just those locations, again for potentially better outflow and success.

Lastly, lymphatic manipulation may assist bleb-related glaucoma surgeries. Opposite to the drug delivery rationale, supporting blebs with increased lymphatics could allow for stronger and longer-lasting bleb function and IOP lowering. This could be pharmacologically induced. Vascular endothelial growth factor (VEGF) is well-known in ophthalmology and

vision science with biologics against it useful to combat new blood vessel growth in various diseases such as macular degeneration (Martin et al., 2011). However, those biologics target VEGF-A and VEGF-B while VEGF-C promotes relatively more lymphatic development (Helotera and Alitalo, 2007). In fact, loss-of-function VEGF-C mutations are known to be associated with lymphedema (Nadarajah et al., 2018). Individual VEGF-C mutations (C156S) (Joukov et al., 1998) even more specifically promote the growth of only lymphatics. VEGF-C has been found in the anterior segment of the eye (Schlereth et al., 2019). Small molecules such as retinoic acid (RA) have also been shown to promote lymphangiogenesis (Choi et al., 2012). After systemic RA delivery, surgical models of hind-limb lymphedema were ameliorated due to lymphatic in-growth (Choi et al., 2012). Thus, various drugs and proteins could be injected into blebs to promote lymphangiogenesis and aqueous outflow. This may be particularly important if anti-fibrotics (such as mitomycin-C or 5-fluorouracil) are toxic to lymphatics. In this case, concurrent injection of anti-fibrotics (to limit scarring) and pro-lymphatic agents (to increase outflow) may simultaneously improve aqueous flow into and out of a bleb.

In conclusion, combining careful and concurrent multi-modal approaches of ocular surface lymphangiography (OSL) with structural assessment and molecular identification, we have confirmed the long-standing hypothesis that lymphatics drain the subconjunctival space. The next steps are to better study subconjunctival outflow to identify the features that allow lymphatic access from blebs. Then, tools need to be developed to suppress or enhance lymphatic function. Applied to drug delivery and glaucoma surgeries, lymphatic manipulation may become a new way to improve ophthalmic clinical care.

Supplementary Material

Refer to Web version on PubMed Central for supplementary material.

Acknowledgements

Funding for this work came from National Institutes of Health, Bethesda, MD (Grant Numbers K08EY024674 [ASH], R01EY030501 [ASH], and R21EY026260 [YH]); AMED (Grant Number JP19am0101078 [YK]; Glaucoma Research Foundation Shaffer Grant [ASH]; Research to Prevent Blindness Career Development Award 2016 [ASH]; an unrestricted grant from Research to Prevent Blindness [UCLA and USC] (New York, NY)

References:

Baluk P, Fuxe J, Hashizume H, Romano T, Lashnits E, Butz S, Vestweber D, Corada M, Molendini C, Dejana E, McDonald DM, 2007 Functionally specialized junctions between endothelial cells of lymphatic vessels. J Exp Med 204, 2349–2362. [PubMed: 17846148]

Barteselli G, Bartsch DU, Viola F, Mojana F, Pellegrini M, Hartmann KI, Benatti E, Leicht S, Ratiglia R, Staurenghi G, Weinreb RN, Freeman WR, 2013 Accuracy of the Heidelberg Spectralis in the alignment between near-infrared image and tomographic scan in a model eye: a multicenter study. Am J Ophthalmol 156, 588–592. [PubMed: 23769196]

Benedikt O, 1976 [Demonstration of aqueous outflow patterns of normal and glaucomatous human eyes through the injection of fluorescein solution in the anterior chamber (author's transl)]. Albrecht Von Graefes Arch Klin Exp Ophthalmol 199, 45–67. [PubMed: 1083684]

Bouhenni RA, Al Jadaan I, Rassavong H, Al Shahwan S, Al Katan H, Dunmire J, Krasniqi M, Edward DP, 2016 Lymphatic and Blood Vessel Density in Human Conjunctiva After Glaucoma Filtration Surgery. J Glaucoma 25, e35–38. [PubMed: 25493624]

Cairns JE, 1968 Trabeculectomy. Preliminary report of a new method. Am J Ophthalmol 66, 673–679. [PubMed: 4891876]

Choi I, Chung HK, Ramu S, Lee HN, Kim KE, Lee S, Yoo J, Choi D, Lee YS, Aguilar B, Hong YK, 2011 Visualization of lymphatic vessels by Prox1-promoter directed GFP reporter in a bacterial artificial chromosome-based transgenic mouse. Blood 117, 362–365. [PubMed: 20962325]

Choi I, Lee S, Kyoung Chung H, Suk Lee Y, Eui Kim K, Choi D, Park EK, Yang D, Ecoiffier T, Monahan J, Chen W, Aguilar B, Lee HN, Yoo J, Koh CJ, Chen L, Wong AK, Hong YK, 2012 9-cis retinoic acid promotes lymphangiogenesis and enhances lymphatic vessel regeneration: therapeutic implications of 9-cis retinoic acid for secondary lymphedema. Circulation 125, 872–882. [PubMed: 22275501]

Freitas-Neto CA, Costa RA, Kombo N, Freitas T, Oréfice JL, Oréfice F, Foster CS, 2015 Subconjunctival indocyanine green identifies lymphatic vessels. JAMA Ophthalmol 133, 102–104. [PubMed: 25275436]

Gaasterland DE, Pederson JE, 1983 Episcleral venous pressure: a comparison of invasive and noninvasive measurements. Invest Ophthalmol Vis Sci 24, 1417–1422. [PubMed: 6618803]

Gedde SJ, Chen PP, Heuer DK, Singh K, Wright MM, Feuer WJ, Schiffman JC, Shi W, Group PTVTS, 2018 The Primary Tube Versus Trabeculectomy Study: Methodology of a Multicenter Randomized Clinical Trial Comparing Tube Shunt Surgery and Trabeculectomy with Mitomycin C. Ophthalmology 125, 774–781. [PubMed: 29248173]

Glauser FL, 1974 Bilateral chemosis and conjunctival venous engorgement in cardiopulmonary failure. Chest 66, 389–394. [PubMed: 4412185]

Gong P, Yu DY, Wang Q, Yu PK, Karnowski K, Heisler M, Francke A, An D, Sarunic MV, Sampson DD, 2018 Label-free volumetric imaging of conjunctival collecting lymphatics ex vivo by optical coherence tomography lymphangiography. J Biophotonics 11, e201800070. [PubMed: 29920959]

Gower EW, Lindsley K, Tulenko SE, Nanji AA, Leyngold I, McDonnell PJ, 2017 Perioperative antibiotics for prevention of acute endophthalmitis after cataract surgery. Cochrane Database Syst Rev 2, CD006364. [PubMed: 28192644]

Green W, Lind JT, Sheybani A, 2018 Review of the Xen Gel Stent and InnFocus MicroShunt. Curr Opin Ophthalmol 29, 162–170. [PubMed: 29319544]

Grüntzig J, Hollmann F, 2019 Lymphatic vessels of the eye - old questions - new insights. Ann Anat 221, 1–16. [PubMed: 30240907]

Guo W, Zhu Y, Yu PK, Yu X, Sun X, Cringle SJ, Su EN, Yu DY, 2012 Quantitative study of the topographic distribution of conjunctival lymphatic vessels in the monkey. Exp Eye Res 94, 90–97. [PubMed: 22138558]

Helotera H, Alitalo K, 2007 The VEGF family, the inside story. Cell 130, 591–592. [PubMed: 17719536]

Huang A, Penteado R, Papoyan V, Voskanyan L, Weinreb R, 2019 Aqueous Angiographic Outflow Improvement after Trabecular Microbypass in Glaucoma Patients. Ophthalmology Glaucoma 2, 11–21. [PubMed: 31595267]

Huang AS, Belghith A, Dastiridou A, Chopra V, Zangwill LM, Weinreb RN, 2017a Automated circumferential construction of first-order aqueous humor outflow pathways using spectral-domain optical coherence tomography. J Biomed Opt 22, 66010. [PubMed: 28617922]

Huang AS, Camp A, Xu BY, Penteado RC, Weinreb RN, 2017b Aqueous Angiography: Aqueous Humor Outflow Imaging in Live Human Subjects. Ophthalmology 124, 1249–1251. [PubMed: 28461013]

Huang AS, Francis BA, Weinreb RN, 2018 Structural and functional imaging of aqueous humour outflow: a review. Clin Exp Ophthalmol 46, 158–168. [PubMed: 28898516]

Huang AS, Kim LA, Fawzi AA, 2012 Clinical characteristics of a large choroideremia pedigree carrying a novel CHM mutation. Arch Ophthalmol 130, 1184–1189. [PubMed: 22965595]

Huang AS, Li M, Yang D, Wang H, Wang N, Weinreb RN, 2017c Aqueous Angiography in Living Nonhuman Primates Shows Segmental, Pulsatile, and Dynamic Angiographic Aqueous Humor Outflow. Ophthalmology 124, 793–803. [PubMed: 28237425]

Huang AS, Mohindroo C, Weinreb RN, 2016a Aqueous Humor Outflow Structure and Function Imaging At the Bench and Bedside: A Review. J Clin Exp Ophthalmol 7.

Huang AS, Saraswathy S, Dastiridou A, Begian A, Legaspi H, Mohindroo C, Tan JC, Francis BA, Caprioli J, Hinton DR, Weinreb RN, 2016b Aqueous Angiography with Fluorescein and Indocyanine Green in Bovine Eyes. Transl Vis Sci Technol 5, 5.

Huang AS, Saraswathy S, Dastiridou A, Begian A, Mohindroo C, Tan JC, Francis BA, Hinton DR, Weinreb RN, 2016c Aqueous Angiography-Mediated Guidance of Trabecular Bypass Improves Angiographic Outflow in Human Enucleated Eyes. Invest Ophthalmol Vis Sci 57, 4558–4565. [PubMed: 27588614]

Huang AS, Weinreb RN, 2017 Structure and Mechanism of Uveoscleral Outflow, in: Francis BA, Sarkisian SR, Tan JC (Eds.), Minimally Invasive Glaucoma Surgery. Thieme, New York, pp. 25–33.

Johnson M, 2006 'What controls aqueous humour outflow resistance?'. Exp Eye Res 82, 545–557. [PubMed: 16386733]

Joukov V, Kumar V, Sorsa T, Arighi E, Weich H, Saksela O, Alitalo K, 1998 A recombinant mutant vascular endothelial growth factor-C that has lost vascular endothelial growth factor receptor-2 binding, activation, and vascular permeability activities. J Biol Chem 273, 6599–6602. [PubMed: 9506953]

Jung E, Gardner D, Choi D, Park E, Jin Seong Y, Yang S, Castorena-Gonzalez J, Louveau A, Zhou Z, Lee GK, Perrault DP, Lee S, Johnson M, Daghlian G, Lee M, Jin Hong Y, Kato Y, Kipnis J, Davis MJ, Wong AK, Hong YK, 2017 Development and Characterization of A Novel Prox1-EGFP Lymphatic and Schlemm's Canal Reporter Rat. Sci Rep 7, 5577. [PubMed: 28717161]

Kato Y, Yamada S, Furusawa Y, Itai S, Nakamura T, Yanaka M, Sano M, Harada H, Fukui M, Kaneko MK, 2019 PMab-213: A Monoclonal Antibody for Immunohistochemical Analysis Against Pig Podoplanin. Monoclon Antib Immunodiagn Immunother 38, 18–24. [PubMed: 30802179]

Khaw P, Grehn F, Holló G, Overton B, Wilson R, Vogel R, Smith Z, Group C-TS, 2007 A phase III study of subconjunctival human anti-transforming growth factor beta(2) monoclonal antibody (CAT-152) to prevent scarring after first-time trabeculectomy. Ophthalmology 114, 1822–1830. [PubMed: 17908591]

Khoo YJ, Abdullah AAH, Yu DY, Morgan WH, 2019 Use of trypan blue to assess lymphatic function following trabeculectomy. Clin Exp Ophthalmol. 47, 892–897. [PubMed: 31074572]

Lama PJ, Fechtner RD, 2003 Antifibrotics and wound healing in glaucoma surgery. Surv Ophthalmol 48, 314–346. [PubMed: 12745005]

Lenzhofer M, Kersten-Gomez I, Sheybani A, Gulamhusein H, Strohmaier C, Hohensinn M, Dick HB, Hitzl W, Eisenkopf L, Sedarous F, Ahmed II, Reitsamer HA, 2018a Four-year results of a minimally invasive transscleral glaucoma gel stent implantation in a prospective multicenter study. Clin Exp Ophthalmol. 47, 581–587.

Lenzhofer M, Strohmaier C, Hohensinn M, Hitzl W, Sperl P, Gerner M, Steiner V, Moussa S, Krall E, Reitsamer HA, 2018b Longitudinal bleb morphology in anterior segment OCT after minimally invasive transscleral ab interno Glaucoma Gel Microstent implantation. Acta Ophthalmol. 97, e231–e237. [PubMed: 30160048]

Martin DF, Maguire MG, Ying GS, Grunwald JE, Fine SL, Jaffe GJ, Group CR, 2011 Ranibizumab and bevacizumab for neovascular age-related macular degeneration. N Engl J Med 364, 1897–1908. [PubMed: 21526923]

Menchini F, Toneatto G, Miele A, Donati S, Lanzetta P, Virgili G, 2018 Antibiotic prophylaxis for preventing endophthalmitis after intravitreal injection: a systematic review. Eye (Lond) 32, 1423–1431. [PubMed: 29891901]

Michael KB, Rotchford A, Ramaesh K, 2016 Conjunctival Chemosis as a Specific Feature of Pseudomonas aeruginosa Corneal Ulcers. Cornea 35, 1182–1184. [PubMed: 27429077]

Nadarajah N, Schulte D, McConnell V, Martin-Almedina S, Karapouliou C, Mortimer PS, Jeffery S, Schulte-Merker S, Gordon K, Mansour S, Ostergaard P, 2018 A Novel Splice-Site Mutation in VEGFC is Associated with Congenital Primary Lymphoedema of Gordon. Int J Mol Sci 19, 2259

Palanca-Capistrano AM, Hall J, Cantor LB, Morgan L, Hoop J, WuDunn D, 2009 Long-term outcomes of intraoperative 5-fluorouracil versus intraoperative mitomycin C in primary trabeculectomy surgery. Ophthalmology 116, 185–190. [PubMed: 18930550]

Pitha I, Oglesby E, Chow A, Kimball E, Pease ME, Schaub J, Quigley H, 2018 Rho-Kinase Inhibition Reduces Myofibroblast Differentiation and Proliferation of Scleral Fibroblasts Induced by Transforming Growth Factor β and Experimental Glaucoma. Transl Vis Sci Technol 7, 6.

Pleyer U, Ursell PG, Rama P, 2013 Intraocular pressure effects of common topical steroids for post-cataract inflammation: are they all the same? Ophthalmol Ther 2, 55–72. [PubMed: 25135807]

Raghava S, Hammond M, Kompella UB, 2004 Periocular routes for retinal drug delivery. Expert Opin Drug Deliv 1, 99–114. [PubMed: 16296723]

Saraswathy S, Tan JC, Yu F, Francis BA, Hinton DR, Weinreb RN, Huang AS, 2016 Aqueous Angiography: Real-Time and Physiologic Aqueous Humor Outflow Imaging. PLoS One 11, e0147176. [PubMed: 26807586]

Schlereth SL, Karlstetter M, Hos D, Matthaei M, Cursiefen C, Heindl LM, 2019 Detection of Pro and Antiangiogenic Factors in the Human Sclera. Curr Eye Res 44, 172–184. [PubMed: 30358460]

Schroedl F, Kaser-Eichberger A, Schlereth SL, Bock F, Regenfuss B, Reitsamer HA, Lutty GA, Maruyama K, Chen L, Lütjen-Drecoll E, Dana R, Kerjaschki D, Alitalo K, De Stefano ME, Junghans BM, Heindl LM, Cursiefen C, 2014 Consensus statement on the immunohistochemical detection of ocular lymphatic vessels. Invest Ophthalmol Vis Sci 55, 6440–6442. [PubMed: 25315233]

Schulte-Merker S, Sabine A, Petrova TV, 2011 Lymphatic vascular morphogenesis in development, physiology, and disease. J Cell Biol 193, 607–618. [PubMed: 21576390]

Shiroma HF, Takaschima AKK, Farah ME, Höfling-Lima AL, de Luca Canto G, Benedetti RH, Rodrigues EB, 2017 Patient pain during intravitreal injections under topical anesthesia: a systematic review. Int J Retina Vitreous 3, 23. [PubMed: 28680703]

Shoukath S, Taylor GI, Mendelson BC, Corlett RJ, Shayan R, Tourani SS, Ashton MW, 2017 The Lymphatic Anatomy of the Lower Eyelid and Conjunctiva and Correlation with Postoperative Chemosis and Edema. Plast Reconstr Surg 139, 628e–637e.

Sohn EH, Wang R, Read R, Roufas A, Teo L, Moorthy R, Albini T, Vasconcelos-Santos DV, Dustin LD, Zamir E, Chee SP, McCluskey P, Smith R, Rao N, 2011 Long-term, multicenter evaluation of subconjunctival injection of triamcinolone for non-necrotizing, noninfectious anterior scleritis. Ophthalmology 118, 1932–1937. [PubMed: 21708408]

Swartz MA, 2014 Immunomodulatory roles of lymphatic vessels in cancer progression. Cancer Immunol Res 2, 701–707. [PubMed: 25092811]

Thach AB, Dugel PU, Flindall RJ, Sipperley JO, Sneed SR, 1997 A comparison of retrobulbar versus sub-Tenon's corticosteroid therapy for cystoid macular edema refractory to topical medications. Ophthalmology 104, 2003–2008. [PubMed: 9400758]

Weinreb RN, 2001 Enhancement of scleral macromolecular permeability with prostaglandins. Trans Am Ophthalmol Soc 99, 319–343. [PubMed: 11797317]

Wong TT, Novack GD, Natarajan JV, Ho CL, Htoon HM, Venkatraman SS, 2014 Nanomedicine for glaucoma: sustained release latanoprost offers a new therapeutic option with substantial benefits over eyedrops. Drug Deliv Transl Res 4, 303–309. [PubMed: 25787063]

Xie X, Akiyama G, Bogarin T, Saraswathy S, Huang AS, 2019 Visual Assessment of Aqueous Humor Outflow. Asia Pac J Ophthalmol (Phila).

Yu DY, Morgan WH, Sun X, Su EN, Cringle SJ, Yu PK, House P, Guo W, Yu X, 2009 The critical role of the conjunctiva in glaucoma filtration surgery. Prog Retin Eye Res 28, 303–328. [PubMed: 19573620]

- Glaucoma bleb-forming surgeries rely upon subconjunctival aqueous outflow.
- Subconjunctival drug delivery is limited by subconjunctival aqueous outflow.
- Subconjunctival outflow is hypothesized to be via lymphatics or blood vessels.
- Structural/molecular imaging demonstrates use of the lymphatic route.
- Better understood, enhancing/minimizing lymphatic outflow may benefit eye care.

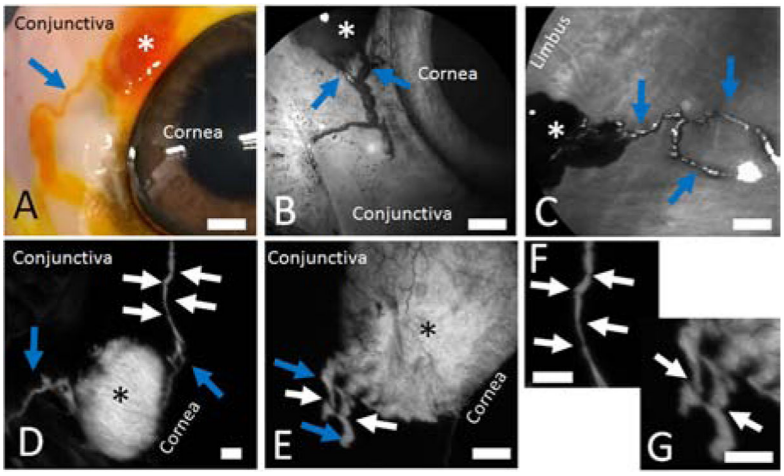

Figure 1.

Distinct Outflow Pathways Can Be Visualized off Blebs Created Using Multiple Tracers in Multiple Species.

In all cases, 100 microliters of a tracer are injected subconjunctival using a 30-gauge needle to create a bleb (asterisks). Distinct outflow pathways are seen arising off of the blebs. A/B/D) Porcine eyes. C) Bovine eye. E) Enucleated right eye from a 54-year-old male. Blue arrows demonstrate outflow pathways. White arrows show intervening regions in the outflow pathways with narrow bands of darker signal. F/G) Zoomed in images of D and E, respectively, showing the dark bands more clearly (white arrows). Scale bars = 1 mm.

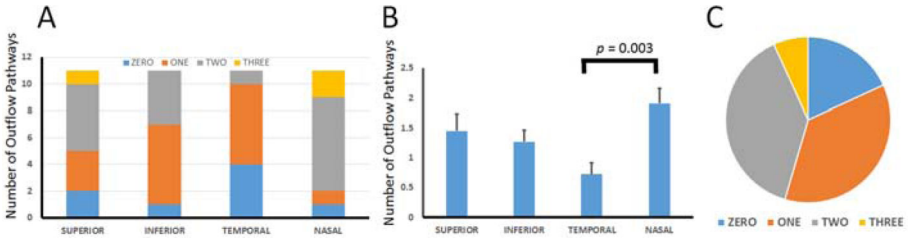

Figure 2.

Variation in Number of Outflow Pathways Off Blebs in Porcine Eyes.

Four separate (superior/inferior/temporal/nasal) 100 microliter subconjunctival blebs were created in each of 11 porcine eyes (n = 44 blebs total), and the number of outflow pathways were counted and compared. A) Each quadrant had a different distribution of total number of pathways seen. B) A statistically significant difference was only seen comparing the temporal to the nasal quadrant. B) The distribution of the number of pathways across all blebs was Zero (18.2%), One (36.4%), Two (38.6%), and Three (6.8%).

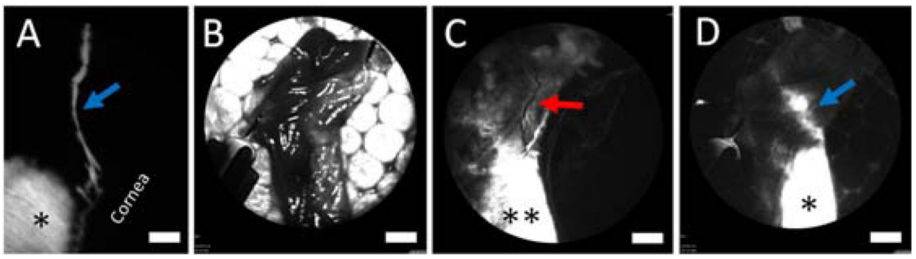

Figure 3.

Outflow Pathways Off Blebs Are Located Within the Conjunctiva of a Porcine Eye.

A) A baseline fluorescent bleb (asterisk) and fluorescent outflow pathway (blue arrow) are apparent. B) To determine the location of this pathway, the conjunctiva from this region was excised and pinned to Styrofoam. C) The residual scleral bed showed fluorescent signal where the bleb was previously located (double asterisks). However, the baseline fluorescent outflow pathway was now gone. Instead a non-fluorescent episcleral vein was seen (red arrow). D) The exact same piece of excised conjunctiva (B) was then imaged with fluorescent excitation showing the bleb (asterisk) and now the fluorescent outflow pathway (blue arrow) again. Scale bars = 1 mm.

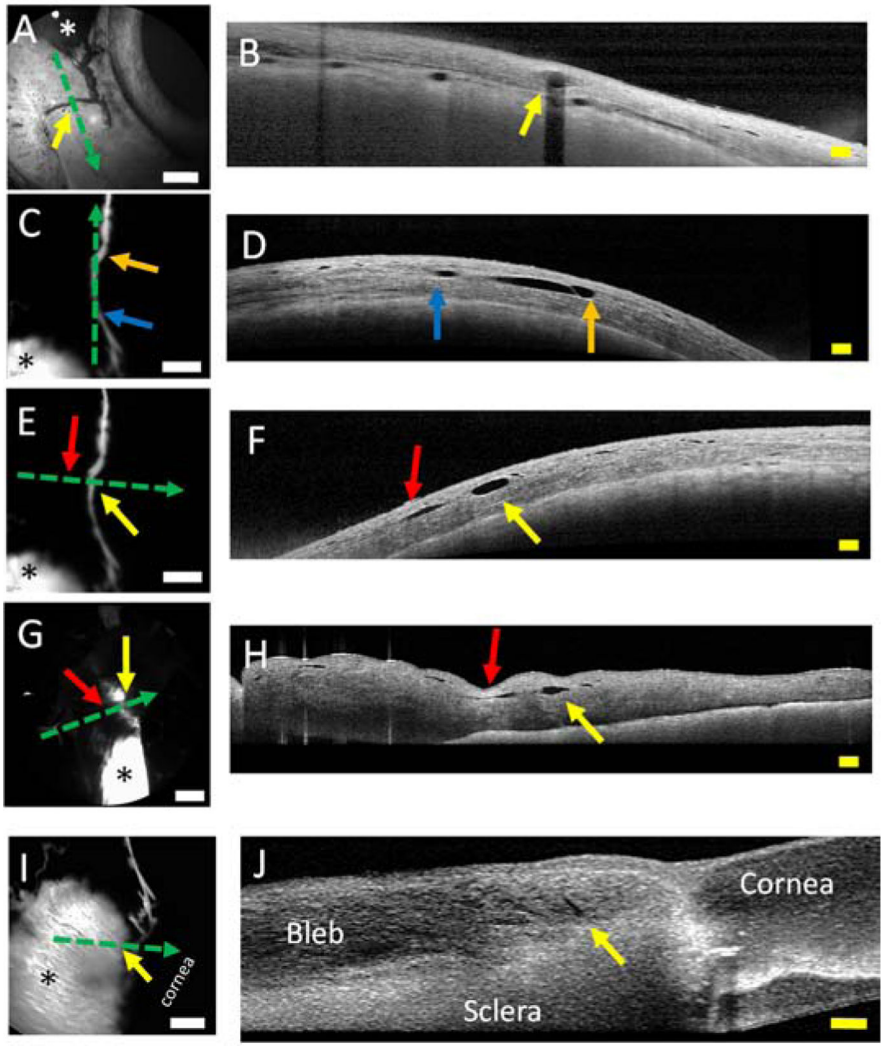

Figure 4.

Structural Evaluation of Outflow Pathways Off Blebs of Porcine Eyes.

Blebs (asterisks) were created with various tracers in porcine eyes, and anterior segment optical coherence tomography (OCT; dotted green arrows) was performed. A/B) OCT transverse to an outflow pathway off the bleb showed a structural lumen. C/D) OCT longitudinal to an outflow pathway from a bleb showed that the extent of the OCT performed on the angiographic outflow pathway matched the extent of the lumen seen on the OCT (blue arrow to orange arrow). E/F) OCT transverse to another outflow pathway from a bleb showed the luminal structure (yellow) arrow. However, next to it was another luminal pathway that did not correspond (red arrow) to an angiographic outflow pathway. G/H) OCT in the exact same location (as E/F) but after the conjunctiva was excised showed the same outflow lumen (yellow arrow) and non-bleb-related outflow lumen (red arrow). I/J) OCT on the junction between the bleb and outflow lumen showed the luminal opening in the bleb (yellow arrow) that could allow fluid to exit from the bleb. White scale bars = 1 mm. Yellow scale bars = 200 microns.

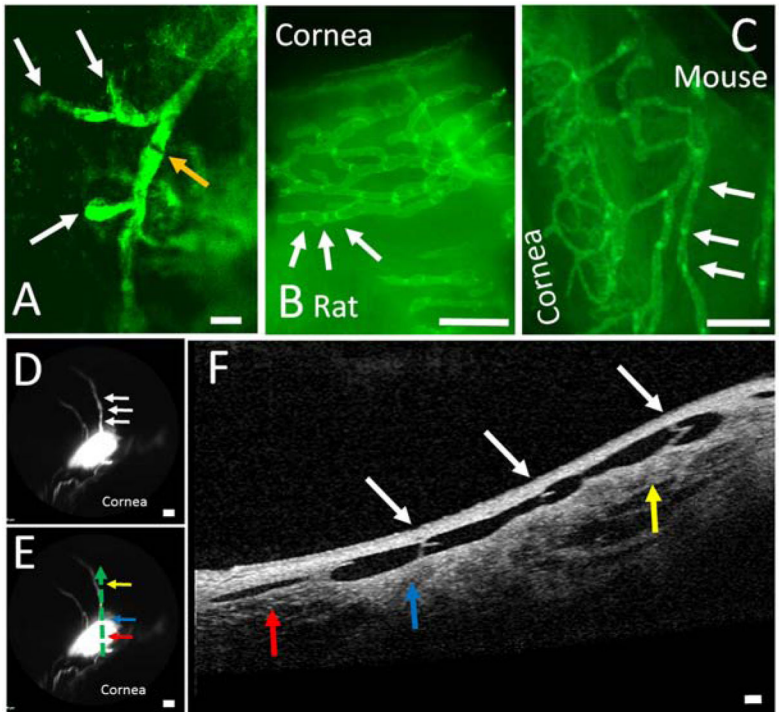

Figure 5.

Structural Characteristics of Outflow Pathways Off Blebs Are Reminiscent of Lymphatics. A) Two-photon microscopy image of fluorescent dextrans trapped in porcine outflow pathways showed structures that are similar to blind-end lymphatics capillaries (white arrow) leading to a possible initial lymphatic trunk with signal variation along the way which may represent valves (orange arrow) (scale bar = 200 microns). This region came from the same tissue as Figure 1D and Figure 3B that included the outflow pathway but not the bleb. Natively fluorescent conjunctival lymphatics are seen from transgenic (B) rat and (C) mouse that expresses EGFP under a Prox-1 promoter. B/C) These lymphatics showed bright spots (white arrows) that are known to represent lymphatic valves (scale bars = 1 mm). D) In a porcine eye, a bleb was created with two outflow pathways arising superior (scale bar = 1 mm). E) OCT was performed and placed on the outflow pathway as denoted by the dotted green arrow with the direction of flow from red to blue to yellow horizontal arrows (scale bar = 1 mm). F) Bicuspid valves (white arrows; that match white arrows in D) are seen in the direction of flow (red to blue to yellow vertical arrows) (scale bar = 100 microns). The red/blue/yellow arrows in (E) match the same colored arrows in (F) and demonstrate a 2-dimensional representation of the outflow pathway off of the bleb.

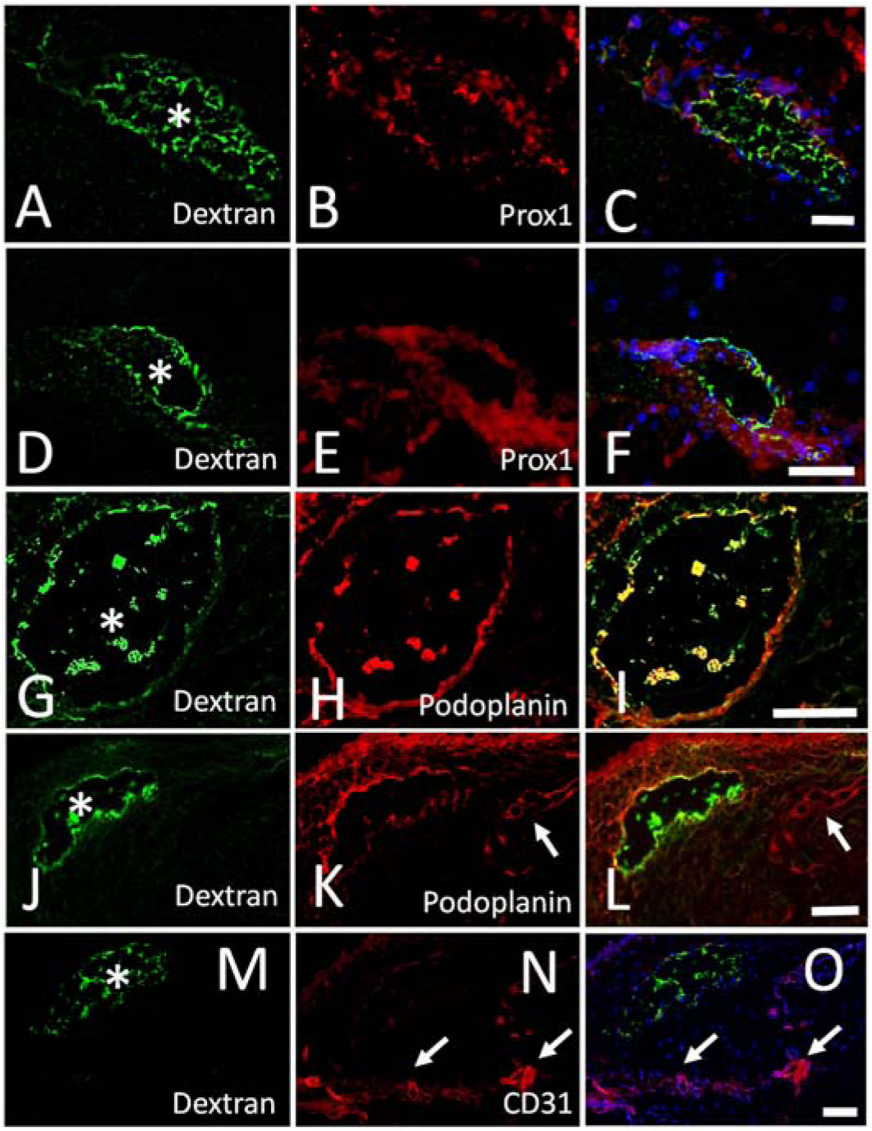

Figure 6.

Outflow Pathways Off Blebs Express Lymphatic Markers in Porcine Eyes.

A/D/G/J/M) After injection of a fluorescent dextran bleb, outflow pathways were seen, fixed, and sectioned. Trapped tracer was seen lining the outflow pathway lumens (white asterisks). A/D) Immunolabeling on the same section against (B/E) Prox-1 showed (C/F) co-localization with the tracer-labeled outflow pathways. G/J) Immunolabeling on the same section against (H/K) podoplanin showed (I/L) co-localization with the tracer-labeled outflow pathways. K/L) Shows images with dextran and podoplanin co-localization but also another lymphatic (white arrow) that did not show tracer labeling. M-O) Immunolabeling on the same section against a blood vessel marker (CD31) did not show co-localization with the tracer-labeled outflow pathway but instead showed distinct blood vessels elsewhere (white arrows). Scale bars = 100 microns.